Blackbox quantization of superconducting circuits using exact impedance synthesis

Firat Solgun,[1,2] David W. Abraham,[3] and David P. DiVincenzo[1,2,4]

[1]*Institute for Quantum Information, RWTH Aachen University, Aachen, Germany*

[2]*Jülich-Aachen Research Alliance, Fundamentals of Future Information Technologies, Germany*

[3]*IBM T.J. Watson Research Center, Yorktown Heights, New York 10598, USA*

[4]*Peter Grünberg Institute: Theoretical Nanoelectronics, Research Center Jülich, Jülich, Germany*

We propose a new quantization method for superconducting electronic circuits involving a Josephson-junction device coupled to a linear microwave environment. The method is based on an exact impedance synthesis of the microwave environment considered as a blackbox with impedance function $Z(s)$. The synthesized circuit captures dissipative dynamics of the system with resistors coupled to the reactive part of the circuit in a nontrivial way. We quantize the circuit and compute relaxation rates following previous formalisms for lumped element circuit quantization. Up to the errors in the fit our method gives an exact description of the system and its losses.

PACS number(s): 03.67.Lx, 42.50.Pq, 85.25.−j

I. INTRODUCTION

The increase in Q factors of superconducting qubits and cavities requires highly accurate models for their design, optimization, and predictability. The common approach to model such systems has been to use Jaynes-Cummings type Hamiltonians borrowed from quantum optics. However, several problems such as convergence issues arise when one wants to include higher levels of superconducting qubits or higher modes of cavities in such models [1].

To remedy those issues a method is proposed in [2] to derive Hamiltonians and compute relaxation rates for superconducting circuits. In this method the linear electromagnetic environment shunting the Josephson junction, as extracted, for example, using microwave simulation software, is lumped together with the junction's linear inductance, to give a "blackbox" impedance function $Z_{\text{sim}}(\omega)$. This response is then fitted, pole by pole, to an analytic function $Z(\omega)$. Then an approximate version of Foster's theorem [3] in the low loss limit [4], applied to $Z(\omega)$, gives an equivalent circuit as a series connection of resonant RLC stages, one stage for each term in the partial fraction expansion of $Z(\omega)$. In this method, which we refer to as the "lossy Foster" method, Q factors for each resonant mode are computed using $Q_p = \frac{\omega_p}{2} \frac{\text{Im}[Y'(\omega_p)]}{\text{Re}[Y(\omega_p)]}$, where $\omega_p = (L_p C_p)^{-1/2}$ and $Y = Z^{-1}$. The lifetime of the mode is given by $T_p = Q_p/\omega_p$.

Lossy Foster, while simple to apply, is not always accurate or even well conditioned. Terms in the partial-fraction expansion of $Z(\omega)$ do not always correspond to stages of a physical circuit [5]. As Brune showed [6], the property that an impedance function must have in order to correspond to a passive physical network is termed "PR (for positive-real)", and this property is an important theme of the present paper. We note that even if all terms in the expansion of $Z(\omega)$ are individually PR one might still need to remove terms by inspection to get a better fit, making the method dependent on *ad hoc* decisions. As applied in [2], lossy Foster parameters are dependent not only on the properties of the electromagnetic environment but also on the precise value of the junction inductance.

In this paper we propose a new method to derive a highly accurate Hamiltonian of a system consisting of a single Josephson junction connected to a linear lossy microwave environment. More general methods for treating fully nonlinear systems, as was done in [7] for one-dimensional (1D) resonator systems, are clearly needed. As in [2], we will focus here on the example involving a transmon qubit coupled to a three-dimensional (3D) microwave cavity. We also treat the electromagnetic environment that the junction sees as a blackbox with an impedance Z_{sim}. To get Z_{sim} we first simulate the cavity system (not including the linear part of the Josephson inductance) and fit the numerical impedance response to a rational function $Z(s)$,

$$Z(s) = \frac{n(s)}{d(s)} = \sum_k \frac{R_k}{s - s_k} + d + es \qquad (1.1)$$

(here s is the Laplace variable), using a well-established technique [8]. We then apply the formalism discovered by Brune [6] to synthesize a circuit that has *exactly* the impedance $Z(s)$ across its terminals. We call the synthesized circuit the "Brune circuit." Since the Brune circuit has a nontrivial topology, we resort to [9,10] to derive its Hamiltonian and compute relaxation rates. Our method, unlike the previous lossy Foster approach [2], involves no approximation in circuit synthesis. Hence the accuracy of our Hamiltonian and dissipation analysis gives an exact description except for very small errors, introduced in fitting, which are inevitable in both approaches.

II. BRUNE SYNTHESIS

After obtaining the rational function fit Eq. (1.1) to $Z(s)$ (details of which are described below), we use results from electrical circuit synthesis theory to obtain a lumped element circuit having exactly this impedance. Brune [6] showed that any impedance response $Z(s)$ satisfying the PR conditions can be realized with a finite passive electric circuit. A scalar impedance function $Z(s)$ is PR if the following two conditions are met.

(1) $Z(s)$ is a rational function which is real for real values of s.

(2) $\text{Re}[Z(s)] \geqslant 0$ for $\text{Re}[s] \geqslant 0$.

The second condition is equivalent to the following.

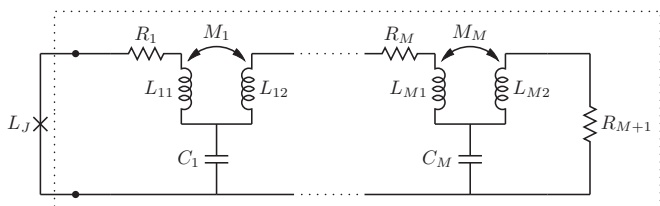(1) No poles lie in the right half plane.

FIG. 1. Brune circuit (in the dotted box) shunted by a Josephson junction. The analysis of this circuit is extensively discussed in Appendix A.

(2) Poles on the j axis have finite positive real residues and are simple.

(3) $\mathrm{Re}[Z(j\omega)] \geqslant 0$.

Indeed, Brune's analysis provides an *algorithm* for finding, without approximation, a lumped element circuit having the PR impedance function $Z(s)$. This extends Foster's original work [3], which applies only to lossless networks.

We apply Brune's algorithm to $Z(s)$, obtaining the lumped circuit of the form shown in Fig. 1. As input, this algorithm for extracting all parameter values of the Brune circuit (Fig. 1) takes the impedance function $Z(s)$ in rational-function form, or (equivalently) partial fraction expansion form. $Y(s) = 1/Z(s)$ can be easily computed in these representations. The algorithm proceeds by looping over the following steps.

(1) If $Z(s)$ or $Y(s)$ has j-axis poles, remove them by realizing terms corresponding to those poles in the partial fraction expansion. Those terms correspond to parallel LC resonators(connected in series) in case of $Z(s)$ poles and series LC resonators (connected in parallel) for $Y(s)$ poles. Repeat until no j-axis pole is left.

(2) Find ω_1 and R_1 such that $R_1 = \min_\omega \mathrm{Re}[Z(j\omega)]$ and $\mathrm{Re}[Z(j\omega_1)] = R_1$. Define $Z_1(s) = Z(s) - R_1$. This step fixes the value of the resistor R_1 in Fig. 2. See Fig. 4 for the degenerate case when $\omega_1 = \infty$.

(3) Define $L_1 = Z_1(j\omega_1)/(j\omega_1)$. If we extract the inductance L_1 as shown in Fig. 2, $1/(Z_1(s) - L_1 s)$ is the admittance corresponding to the rest of the circuit and has a pole at $s = j\omega_1$, and hence we can write

$$\frac{1}{Z_1(s) - L_1 s} = \frac{(1/L_2)s}{s^2 + \omega_1^2} + \frac{1}{W(s)}. \tag{2.1}$$

(4) The first term in Eq. (2.1) corresponding to the pole at $s = j\omega_1$ is realized with a shunt LC branch consisting of inductance L_2 connected in series with capacitance $C_2 = 1/(L_2\omega_1^2)$ as shown in Fig. 2.
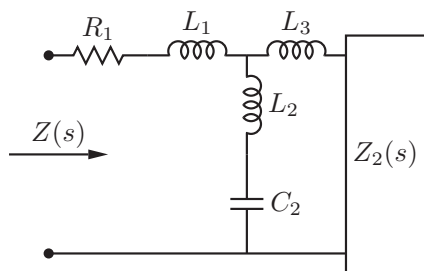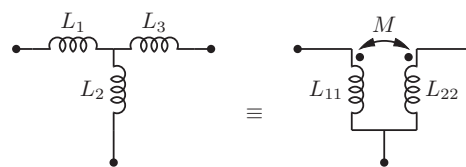

FIG. 2. Brune circuit extraction step.

FIG. 3. Equivalence of a T-shaped inductive circuit in Fig. 2 to a coupled inductor.

(5) $W(s)$ has a pole at infinity such that

$$\lim_{s \to \infty} W(s) = -\frac{L_1 L_2 s}{L_1 + L_2} = L_3 s. \tag{2.2}$$

This pole is removed by constructing $Z_2(s) = W(s) - L_3 s$, which corresponds to connecting in series an inductance of value $L_3 = -L_1 L_2/(L_1 + L_2)$. $Z_2(s)$ is PR, and one loops though steps 1–5 applied to Z_2.

Steps 1 to 5 reduce degrees of both numerator and denominator of $Z(s)$ by 2 so that the algorithm terminates once a constant $Z_2(s) = R_{M+1}$ is reached. For more details on Brune's algorithm see [5].

The circuit in Fig. 2 involves negative values for either inductance L_1 or L_3 [5]. However, one can replace the T-shaped inductive part of the circuit in Fig. 2 with a "tightly coupled" inductor as shown in Fig. 3, where the inductances are all physically realizable and given by

$$L_{11} = L_1 + L_2, \tag{2.3}$$

$$L_{22} = L_3 + L_2, \tag{2.4}$$

$$M = L_2. \tag{2.5}$$

Note that lower terminals of the coupled inductor are short circuited.

Note that at any stage in the application of step 2, above, one may find $\omega_1 = 0$ or ∞. In case of $\omega_1 = \infty$ we have the degenerate circuit in Fig. 4 which corresponds to the circuit in Fig. 3 with $L_1 = L_2 = L_3 = 0$. C_j in Fig. 4 is given by

$$C_j = \lim_{s \to \infty} \frac{1}{s(Z_j - R_j)}. \tag{2.6}$$

Brune's circuit consists of M stages, each of which generally contains a tightly coupled inductor pair ($M_j = \sqrt{L_{j1}L_{j2}}$), a capacitor C_j, and a series resistor R_j. As shown below, this interleaving of M lossless stages with $(M + 1)$ resistors results in nontrivial coupling between modes of the circuit and the dissipative environment represented by these resistors.
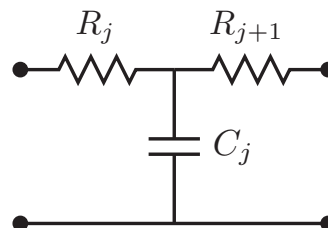

FIG. 4. A degenerate stage in a Brune circuit.

III. CIRCUIT QUANTIZATION

We quantize the Brune circuit following the formalism of [10]; this reference and [9] also provide variants of the standard treatment of resistors, which we will use here, as a bath of harmonic oscillators with a smooth frequency spectrum, as developed initially by Caldeira and Leggett. We derive a Lagrangian $\mathcal{L}_S$ (or equivalently a Hamiltonian $\mathcal{H}_S$) corresponding to a 1D chain of interacting oscillator degrees of freedom (details may be found in Appendix A):

$$\mathcal{L}_S = \tfrac{1}{2}\dot{\boldsymbol{\Phi}}^T \mathcal{C}\dot{\boldsymbol{\Phi}} - U(\boldsymbol{\Phi}), \quad \mathcal{H}_S = \tfrac{1}{2}\boldsymbol{Q}^T\mathcal{C}^{-1}\boldsymbol{Q} + U(\boldsymbol{\Phi}), \quad (3.1)$$

where

$$U(\boldsymbol{\Phi}) = -\left(\frac{\Phi_0}{2\pi}\right)^2 L_J^{-1}\cos(\varphi_J) + \frac{1}{2}\boldsymbol{\Phi}^T\mathbf{M_0}\boldsymbol{\Phi}. \quad (3.2)$$

Here $\boldsymbol{\Phi}$ is a vector of length $(M+1)$ whose first coordinate is proportional to the phase across the Josephson junction $\Phi_1 = (\frac{\Phi_0}{2\pi}\varphi_J)$ [in case of a single capacitive degenerate stage, $\boldsymbol{\Phi}$ is of length M (see Appendix A)]. There is a local relationship between the new coordinates and the branch flux variables in the original Brune circuit in Fig. 1 [see Eqs. (A16)–(A25) in Appendix A for details]:

$$\Phi_{j1} = (-1)^{j+1}\frac{t_j}{1-t_j}(\Phi_j + \Phi_{j+1}), \quad (3.3)$$

$$\Phi_{j2} = (-1)^{j}\frac{1}{1-t_j}(\Phi_j + \Phi_{j+1}), \quad (3.4)$$

for $1 \leqslant j \leqslant M$, with $t_j = \sqrt{\frac{L_{j1}}{L_{j2}}}$, where Φ_{j1} and Φ_{j2} are the fluxes across the left and right branches of coupled inductors in the Brune circuit in Fig. 1.

The chain structure of our representation is evident in the tridiagonality of the capacitance and inverse inductance matrices:

$$\mathcal{C} = \begin{pmatrix} C_1' & t_1 C_1' & & & \\ t_1 C_1' & t_1^2 C_1' + C_2' & \ddots & & \mathbf{0} \\ & \ddots & \ddots & & \\ \mathbf{0} & & & t_{M-1}^2 C_{M-1}' + C_M' & t_M C_M' \\ & & & t_M C_M' & t_M^2 C_M' \end{pmatrix}, \quad (3.5)$$

$$\mathbf{M_0} = \begin{pmatrix} \frac{1}{L_1'} & \frac{1}{L_1'} & & & \\ \frac{1}{L_1'} & \frac{1}{L_1'} + \frac{1}{L_2'} & \ddots & & \mathbf{0} \\ & \ddots & \ddots & & \\ \mathbf{0} & & & \frac{1}{L_{M-1}'} + \frac{1}{L_M'} & \frac{1}{L_M'} \\ & & & \frac{1}{L_M'} & \frac{1}{L_M'} \end{pmatrix}, \quad (3.6)$$

$C_j' = C_j/(1-t_j)^2$, $L_j' = L_{j2}(1-t_j)^2$.

Applying Eq. (124) of [9] we get the contribution to the relaxation rate from the resistor R_j ($1 \leqslant j \leqslant M+1$):

$$\frac{1}{T_{1,j}} = 4|\langle 0|\bar{\mathbf{m}}_j \cdot \boldsymbol{\Phi}|1\rangle|^2 J_j(\omega_{01})\coth\left(\frac{\hbar\omega_{01}}{2k_B T}\right). \quad (3.7)$$
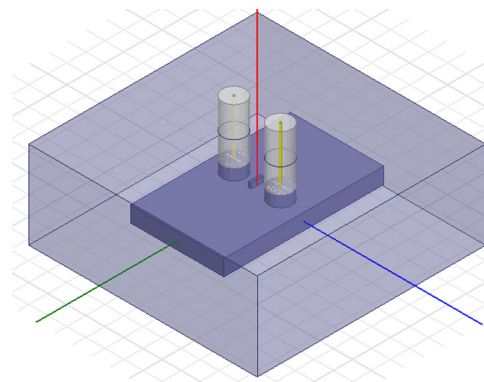

FIG. 5. (Color online) Geometry of the 3D transmon qubit simulated in HFSS. The light blue color indicates the perfect conductor, and the dark blue color indicates the vacuum. The qubit port terminals are defined on a dielectric substrate located at the position of the red line. Two coaxial ports are positioned symmetrically on each side of the substrate. The cavity dimensions are (height, length, width) = (4.2, 24.5, 42 mm).

$|0,1\rangle$ are the qubit eigenlevels of the system Hamiltonian Eq. (3.1), and ω_{01} is the transition frequency between them. Calculating these quantities requires solving the Schrödinger equation for the system Hamiltonian above; this can be a difficult task, but many effective accurate methods have been developed for doing this, in many works right up to the present [9–11,27]. The vector $\bar{\mathbf{m}}_j$ [of length $(M+1)$] describes the coupling of the system to the environment representing resistor R_j; for our Brune circuit this is, for $1 \leqslant j \leqslant M$,

$$\bar{\mathbf{m}}_j = \begin{pmatrix} 0 \\ \vdots \\ 0 \\ \frac{(-1)^{j-1}C_j}{(1-t_j)} \\ \frac{(-1)^{j}C_{j+1}}{(1-t_{j+1})} + \frac{(-1)^{j-1}t_j C_j}{(1-t_j)} \\ \vdots \\ \frac{(-1)^{M-1}C_M}{(1-t_M)} + \frac{(-1)^{M-2}t_{M-1}C_{M-1}}{(1-t_{M-1})} \\ \frac{(-1)^{M-1}t_M C_M}{(1-t_M)} \end{pmatrix}. \quad (3.8)$$
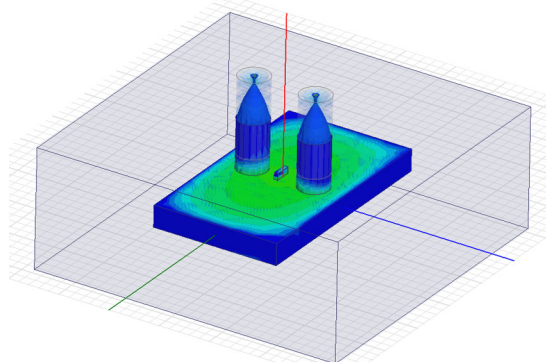

FIG. 6. (Color online) Fundamental mode (the TE101 mode) of the cavity with frequency $f_{\mathrm{TE101}} = 6.875$ GHz. The green color indicates electric-field regions of higher magnitude compared to blue regions.

TABLE I. Poles and residues for the fit to the HFSS dataset for Z_{sim} as in the second part of Eq. (1.1).

k	Pole s_k (GHz)	Residue R_k
1	-1.6152×10^{-6}	8363.13
2,3	$-0.001\,103\,72 \pm j6.874\,73$	$5.696\,12 \pm j0.003\,692\,73$
4,5	$-0.006\,717\,33 \pm j7.057\,11$	$(6.266\,09 \pm j1.341\,64) \times 10^{-5}$
6,7	$-1.349\,01 \pm j8.984\,53$	$(7.332\,83 \pm j5.615\,51) \times 10^{-3}$
8,9	$-0.002\,727\,01 \pm j12.0048$	$7.151\,59 \pm j0.022\,788\,2$
10,11	$-0.009\,186\,35 \pm j12.8561$	$(1.986\,02 \pm j0.013\,499\,6) \times 10^{-3}$
12,13	$-1.402\,14 \pm j13.7644$	$(-8.608\,07 \pm j9.403\,97) \times 10^{-3}$
14,15	$-0.131\,778 \pm j17.7404$	$23.8075 \pm j1.174\,04$
16,17	$-3.149\,27 \pm j88.3524$	$(1.195\,27 \pm j0.120\,033) \times 10^4$

The spectral density corresponding to the bath representing R_j is

$$J_j(\omega) = \omega^3 R_j \left[1 + \omega^2 R_j^2 \left(\sum_{k=j}^{M} C_k \right)^2 \right]^{-1}. \quad (3.9)$$

For the last resistor R_{M+1}, $\bar{\mathbf{m}}_{M+1} = (0 \cdots 0\,1)^T$, and $J_{M+1}(\omega) = \omega/R_{M+1}$.

IV. EXAMPLE

To show the application of the synthesis method we have just described, we analyze a dataset produced to analyze a 3D transmon similar to the one reported in a recent experiment at IBM [12]. Our modeling is performed using the finite-element electromagnetics simulator HFSS (for High Frequency Structural Simulator) [13]. Since the systems we want to model admit very small loss [14,15], they are very close to the border which separates passive systems from active ones. Therefore it is necessary to take care that the simulation resolution is high enough to ensure the passivity of the simulated impedance. Otherwise the fitted impedance $Z(s)$ does not satisfy the PR conditions [6], meaning that there is no passive physical network corresponding to $Z(s)$.

The simulated device is a 3D transmon, inserted with appropriate antenna structures into the middle of a rectangular superconducting (aluminium) box cavity, which is standard in several laboratories presently for high-coherence qubit experiments. Figure 5 shows a perspective rendering of the device, and Fig. 6 shows an intensity map of the fundamental

mode of the cavity. The simulation includes two coaxial ports entering the body of the cavity symmetrically on either side of the qubit. HFSS is used to calculate the device's three-port S matrix over a wide frequency range, from 3.0 to 15.0 GHz. The three ports are those defined by the two coaxial connectors and the qubit terminal pair. That is, the metal defining the Josephson junction itself is absent from the simulation, so that its very small capacitance and (nonlinear) inductance can be added back later as a discrete element as in Fig. 1. The conversion from the S matrix to Z_{sim} is calculated using standard formulas [16,17], in which it is assumed that the two coaxial ports are terminated with a matched ($Z_0 = 50\ \Omega$) resistor. We have confirmed that the lossy part of the resulting impedance is mostly determined by these port terminations, rather than by the (physically rather inaccurate) HFSS model of cavity-metal losses; this is consistent with the Q of the system being determined by its external couplings [12].

To obtain the fitted rational impedance function $Z(s)$ as in Eq. (1.1), we use the MATLAB package Vector Fitting (VF) [8]. Vector Fitting is an algorithm to approximate a sampled impedance or admittance response by a rational function. It takes a dataset over sampled frequency points, and the number of poles M required for the fit, as its input and gives a set of poles and residues as its output (see [18] for models with an infinite number of poles). Reference [19] discusses details of VF. Its passivity enforcement subroutine [20] makes sure that the real part of the resulting rational approximation is positive definite. This feature is crucial for our analysis since we require the impedance response to be PR for the existence of a finite passive network having the same impedance across its terminals. Note that passivity enforcement may not always

TABLE II. Parameter values for the synthesized Brune circuit. Note the strong (orders of magnitude) increase in impedance (in R and $\sqrt{L/C}$ values) as we go deep in the circuit. The fifth stage is degenerate, treated in more detail in Appendix A.

i	R_i	C_i (nF)	L_{i1} (nH)	L_{i2} (nH)
1	$5.719\,74 \times 10^{-5}$	$1.170\,20 \times 10^{-4}$	$1.328\,10 \times 10^{-1}$	$3.020\,58 \times 10^{1}$
2	$5.531\,99 \times 10^{-2}$	$2.490\,81 \times 10^{-6}$	$8.752\,72 \times 10^{1}$	$3.742\,25 \times 10^{3}$
3	$1.840\,87 \times 10^{2}$	$6.017\,27 \times 10^{-8}$	$4.129\,54 \times 10^{3}$	$1.981\,21 \times 10^{4}$
4	$1.790\,21 \times 10^{4}$	$1.441\,53 \times 10^{-9}$	$4.560\,24 \times 10^{4}$	$2.674\,89 \times 10^{5}$
5*	$6.571\,08 \times 10^{5}$	$2.019\,06 \times 10^{-10}$	0	0
6	$4.900\,91 \times 10^{5}$	$9.699\,33 \times 10^{-12}$	$1.561\,73 \times 10^{7}$	$1.554\,36 \times 10^{7}$
7	$4.146\,78 \times 10^{7}$	$1.640\,15 \times 10^{-12}$	$3.098\,21 \times 10^{8}$	3.1134×10^{8}
8	$2.337\,93 \times 10^{7}$	$6.320\,07 \times 10^{-11}$	$4.741\,68 \times 10^{6}$	$1.951\,74 \times 10^{6}$
9	$1.223\,42 \times 10^{8}$	$1.705\,36 \times 10^{-11}$	$7.423\,02 \times 10^{6}$	$1.106\,08 \times 10^{7}$
10	$6.357\,12 \times 10^{8}$			

work if the accuracy of the microwave simulation is not high enough, and we have taken care to run the simulation with suitably high resolution.

Applying VF to Z_{sim} gives the partial fraction expansion form in Eq. (1.1) with the poles s_k and residues R_k listed in Table I, with $e = 0$ and $d = 2.804\,07\ \Omega$. We fixed the number of poles M by increasing M until VF could not improve the fit further, stopping at $M = 17$. Note that some of the poles obtained in the fit have frequencies (the imaginary part of s_k) outside the range of the simulation data; this is a normal feature of the fitting routine, used to guarantee a highly accurate fit throughout the entire simulated frequency band.

We have applied both Brune's algorithm and a lossy Foster analysis to our fitted $Z(s)$. Circuit parameters obtained for the Brune circuit are listed in Table II. We see that the series resistor connected directly to the qubit is quite tiny—the qubit is nearly lossless. The progressive increase of the resistance values in further stages of the circuit does not imply a large contribution of these resistors to loss, as they are seen by the qubit only through a kind of LC "filter." Indeed, the strong trend toward increasing impedance from stage to stage in the Brune network (both in the R and $\sqrt{L/C}$ values) means that the first few stages of the Brune network already give a good approximation of the cavity response $Z(s)$.

In fitting our data with the lossy Foster method (see Appendix B) one must be careful about residues with negative real parts or significant imaginary parts. Note that one cannot apply the lossy Foster approximation to terms corresponding to poles 12 and 13 in Table I since they have residues with negative real parts—there is no physical network to approximate those terms alone. We also drop dc and high-frequency terms corresponding to poles 1 and 14–17 respectively: such a choice gives a better approximation for the real part of the impedance in the frequency band of interest. Thus, the best approximating Foster network consists of five RLC stages, representing the ten remaining pole pairs.

In Fig. 7 we compare these open circuit impedances, as represented by the Brune and lossy Foster methods, over the full range of our simulation data. The Foster representation
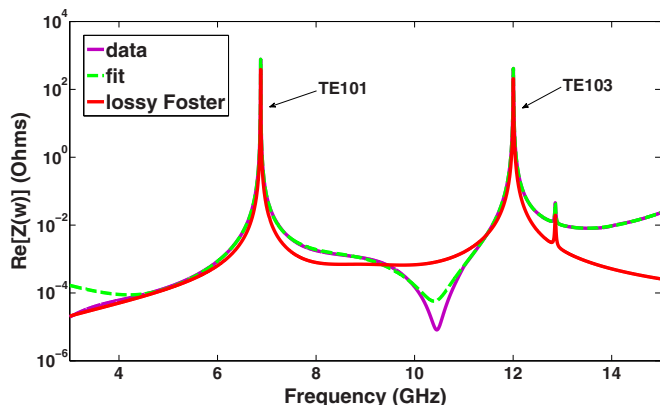

FIG. 7. (Color online) Real part of the open circuit response. The dotted green line indicates the open circuit response for the Brune circuit which we identify with the open circuit fit. The solid magenta line indicates the simulated response. The red line indicates the response of the lossy Foster circuit. TE101 and TE103 are the resonances associated with classical rectangular cavity modes [21].
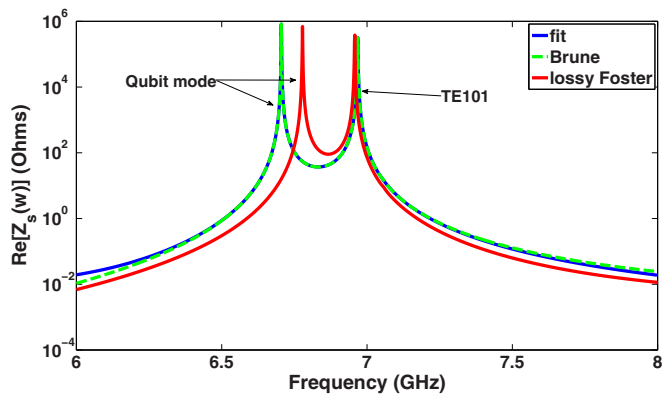

FIG. 8. (Color online) Real part of impedance in a small range of frequencies around the qubit pole ($f_{\text{qb}} = 6.7052$ GHz, where f_{qb} is the qubit resonance for the exact fit) for the system shunted (with impedance Z_s) by a linear inductance $L_J = 4.5$ nH representing the Josephson junction for three different cases. The TE101 mode is not strongly affected by the presence of L_J.

clearly captures the main features of the response, notably the two classical box resonances of the cavity. However, in finer detail, especially far away from the resonances, the Brune representation, which is essentially indistinguishable from the fit obtained from VF, matches much better than the best lossy Foster circuit.

We now show the improvements that can be expected by using the Brune circuit when representing the dynamics of the qubit-cavity system. Here we perform only simple calculations involving a harmonic qubit [22] (i.e., one represented by a linear inductance L_J), but our results give evidence that the Brune circuit will provide high-quality predictions even for more complex, strongly anharmonic qubits. In Fig. 8 we show the lossy part of the impedance when the cavity is shunted by a linear inductance $L_J = 4.5$ nH. The fundamental cavity
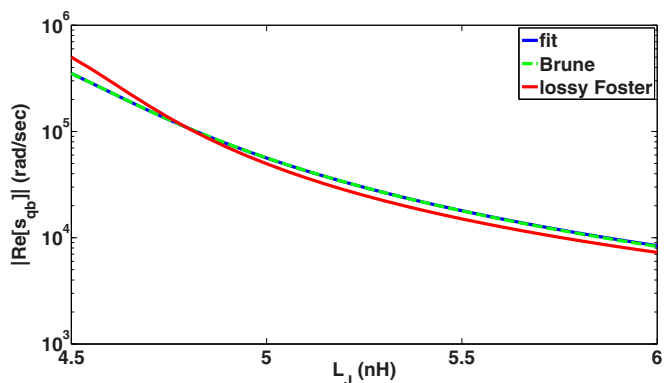
FIG. 9. (Color online) Magnitude of the real part of qubit pole s_{qb} as a function of linear inductance representing the Josephson junction shunting the system for three different cases: the exact fit for the system shunted by the linear inductance, the Brune circuit shunted by the linear inductance, and the lossy Foster circuit shunted by the linear inductance. The overall decreasing trend of this rate is simply due to the movement of the qubit pole to decreasing frequency as L_J is increased. The T_1 relaxation rate of the qubit is given by $T_1^{-1} = \omega_{\text{qb}}/Q_{\text{qb}}$, where the quality factor $Q_{\text{qb}} = \omega_{\text{qb}}/|\xi_{\text{qb}}|$ with $\xi_{\text{qb}} = \text{Re}[s_{\text{qb}}]$ and $\omega_{\text{qb}} = \text{Im}[s_{\text{qb}}]$ is the frequency of the qubit mode.
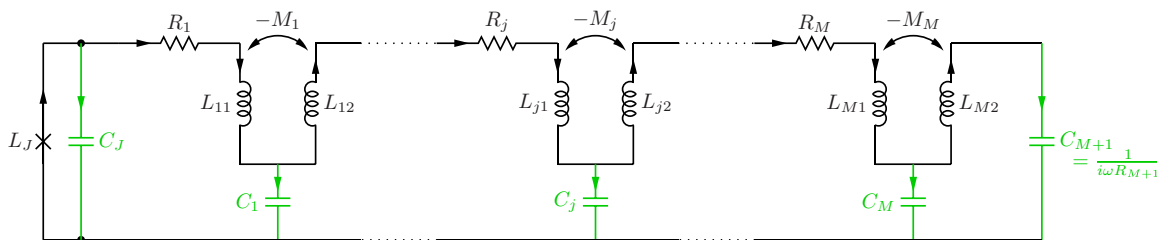
FIG. 10. (Color online) Modified Brune circuit. Tree branches are shown in black, and chord branches are shown in green. Current directions are chosen to have the matrix $\mathcal{F}_C$ in Eq. (A1) with all positive entries. Formal capacitance C_{M+1} is introduced for a technical reason: with the substitution $C_{M+1} = \frac{1}{i\omega R_{M+1}}$ we are able to compute the dissipation rate due to R_{M+1} in the formalism of [9]. After the coordinate transformations we take the $C_J \to 0$ limit. To get $\mathcal{F}_C$ in Eq. (A1) with all positive entries we reversed the direction of currents through and inverted the polarity of voltages across right coupled inductor branches, which requires the update $M_j \to -M_j$ for mutual inductances. See Fig. (13) for the definition of the coupled inductor.

resonance (TE$_{101}$) is not significantly changed from the open circuit case, but the qubit appears as a new pole in the response. This "qubit pole" is again very accurately represented by the Brune circuit [23]; however, using the lossy Foster circuit derived from the open circuit case above, the qubit pole is significantly misplaced, by about 100 MHz.

Of course, in current applications of the Foster approach [2], one can do much better by refitting the Foster form with the linear inductance included in the response, and thus adding a new RLC stage to explicitly represent the qubit pole. This is an effective strategy [24], but the results in Fig. 9 will indicate its limitations.

Here we compare the use of the Brune and (fixed) lossy Foster circuit in giving the real part of the qubit pole, which is proportional to the relaxation rate $1/T_1$ [Eq. (3.7)], as the inductance L_J is varied. We see again that the Brune circuit matches the "fit" result, obtained directly from the HFSS data, very closely. The deviations of the lossy Foster result are up to 20%, and the decrease of the loss rate with L_J is significantly underestimated. This suggests that no single lossy Foster network, incorporating some fixed amount of linear inductance, will be able to match this trend.

Thus, while the Foster approach has been of considerable value in modeling nearly harmonic qubits like transmons [2], it appears that the exactness of the Brune approach will be of real value as we consider other more anharmonic cavity-coupled qubits. A clear application in this direction will be the cases of fluxonium [25] or flux qubits [26]— our approach should provide a highly accurate multimode Hamiltonian for modeling dynamics in those cases. As we move also to multiqubit multiport modeling problems, we are hopeful that application of further electrical theories, developed actively for problems of network synthesis in the decades after Brune's work, will prove very useful in providing new modeling techniques for contemporary quantum computer devices.

APPENDIX A: QUANTIZATION OF THE BRUNE CIRCUIT

In this section we present a full derivation (based on the formalism in [9,10]) of the Brune circuit Hamiltonian and relaxation rate expressions.

An augmented form of the Brune circuit is shown in Fig. 10. The last resistor R_{M+1} is replaced with a capacitor C_{M+1}. It will be included in our analysis later through the substitution $C_{M+1} \leftarrow 1/(i\omega R_{M+1})$. The lossless part of this circuit as used to construct the system Hamiltonian in the main text is shown in Fig. 11; the construction of Fig. 12 shows that in the special case of the unity turns ratio this circuit is exactly the (dual) lossless Foster form.

We will compute its dissipative effect referring to the equation of motion Eq. (61) in [9]. We also add a formal capacitance C_J shunting the Josephson junction. This is required for a nonsingular capacitance matrix if there are no degenerate stages. Coupled inductors in the circuit in Fig. 10 satisfy "tight" coupling condition $M_j = \sqrt{L_{j1}L_{j2}}$. The
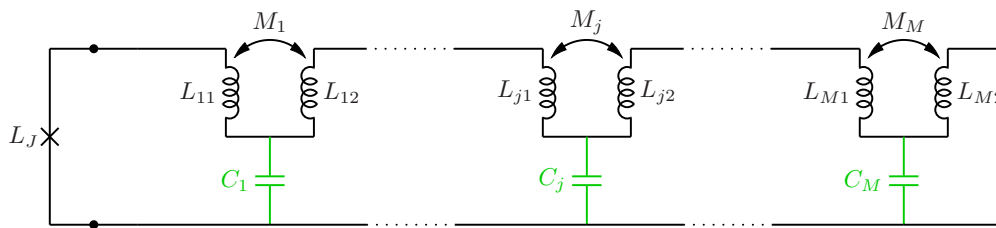
FIG. 11. (Color online) Lossless part of the Brune circuit. It is this circuit that is described by the "system" Hamiltonian Eqs. (3.1) and (3.2). As discussed above, we take the limit $C_J \to 0$ so that this element is removed. The lossless circuit is obtained from Fig. 10 by taking $R_1, R_2, \ldots R_M \to 0$ and $R_{M+1} \to \infty$. It is these different limiting treatments that require that the descriptions of $R_1 - R_M$ follow the low-impedance treatment as in [10], while the description of R_{M+1} needs the high-impedance treatment as in [9].

FIG. 12. Circuit identity showing that tightly coupled inductor pairs simplify in the case of a turns ratio equal to 1; in this case Fig. 11 becomes identical to one of the classic lossless Foster canonical forms [3,5].

inductance matrix L_t in Eq. (15) of [10] becomes singular in the tight coupling limit. To remedy this issue we will rotate coordinates to eliminate half of the degrees of freedom corresponding to coupled inductor branches. With the ordering $(L_J, L_{12}, L_{22}, \ldots, L_{M2}, L_{11}, L_{21}, \ldots, L_{M1}, R_1, \ldots, R_M)$ and $(C_J, C_1, \ldots, C_M, C_{M+1})$ for tree and chord branches, respectively (note that right coupled inductor branches come first and that there are no chord inductors), we construct the $\mathcal{F}_C$ matrix in Eq. (21) of [10]:

$$\mathcal{F}_C = \begin{pmatrix} 1 & 1 & 1 & \cdots & 1 & 1 \\ & 1 & \cdots & 1 & 1 \\ & & \ddots & \vdots & \vdots \\ & & 0 & & 1 & 1 \\ & & & & & 1 \\ 0 & 1 & 1 & \cdots & 1 & 1 \\ & 1 & \cdots & 1 & 1 \\ & & \ddots & \vdots & \vdots \\ & & 0 & & 1 & 1 \end{pmatrix}, \quad (A1)$$

where $\mathcal{F}_C$ is a $(2M+1) \times (M+2)$ matrix. To get $\mathcal{F}_C$ with all positive entries we reversed the direction of currents through and inverted the polarity of voltages across right coupled inductor branches, which requires the update $M_j \rightarrow -M_j$ for mutual inductances. See Fig. 10 for directions of branch currents and Fig. 13 for the definition of the coupled inductor. A generic two-port coupled inductor is shown in Fig. 13 with the following constitutive relations:

$$\begin{pmatrix} \Phi_1 \\ \Phi_2 \end{pmatrix} = \begin{pmatrix} L_{11} & M \\ M & L_{22} \end{pmatrix} \begin{pmatrix} I_1 \\ I_2 \end{pmatrix}, \quad (A2)$$
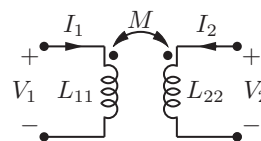
FIG. 13. Generic two-port coupled inductor with the convention chosen for current directions and voltage polarities.

assuming the conventions shown in Fig. 13 for current directions and voltage polarities. With the current directions chosen the stored energy in the coupled inductor is given by

$$E = \tfrac{1}{2}(L_{11}I_1 + 2M I_1 I_2 + L_{22}I_2). \quad (A3)$$

We compute the capacitance matrix in Eq. (22) of [10] as

$$\mathcal{C}_0 = \mathcal{F}_C C \mathcal{F}_C^t, \quad (A4)$$

where C is the diagonal matrix with capacitances $(C_J, C_1, \cdots, C_M, C_{M+1})$ in the diagonal. With the directions chosen for coupled inductor currents, L_t^{-1} in Eq. (16) of [10] is written as

$$L_t^{-1} = \frac{1}{L_0^2} \begin{pmatrix} L_{11} & & 0 & M_1 & & 0 \\ & \ddots & & & \ddots & \\ 0 & & L_{M1} & 0 & & M_M \\ M_1 & & 0 & L_{12} & & 0 \\ & \ddots & & & \ddots & \\ 0 & & M_M & 0 & & L_{M2} \end{pmatrix}, \quad (A5)$$

where $M_j = \sqrt{L_{j1}L_{j2} - L_0^2}$, with $L_0 > 0$ being a small parameter giving the deviation from the tight coupling limit. We have

$$\mathcal{G} = \begin{pmatrix} 0 \\ 1_{2M \times 2M} \end{pmatrix} \quad (A6)$$

and

$$M_0 = \mathcal{G} L_t^{-1} \mathcal{G}^t \quad (A7)$$

$$= \begin{pmatrix} 0 & 0 \\ 0 & L_t^{-1} \end{pmatrix}. \quad (A8)$$

We construct a rotation matrix U:

$$U = \begin{pmatrix} 1 & 0 & & \cdots & & & 0 \\ 0 & \frac{1}{\sqrt{1+t_1^2}} & & 0 & \frac{t_1}{\sqrt{1+t_1^2}} & & 0 \\ & & \ddots & & & \ddots & \\ \vdots & 0 & & \frac{1}{\sqrt{1+t_M^2}} & 0 & & \frac{t_M}{\sqrt{1+t_M^2}} \\ & -\frac{t_1}{\sqrt{1+t_1^2}} & & 0 & \frac{1}{\sqrt{1+t_1^2}} & & 0 \\ & & \ddots & & & \ddots & \\ 0 & 0 & & -\frac{t_M}{\sqrt{1+t_M^2}} & 0 & & \frac{1}{\sqrt{1+t_M^2}} \end{pmatrix}, \quad (A9)$$

where $t_j = \sqrt{\frac{L_{j1}}{L_{j2}}}$. We now compute $U^t M_0 U$ and truncate it to its upper-left $(M+1) \times (M+1)$ sector (by taking the $L_0 \to 0$ limit), which corresponds to the eigenspace with finite (noninfinite) eigenvalues. After truncation we get

$$
M_0' = \begin{pmatrix} 0 & & & 0 \\ & 1/L_1 & & \\ & & \ddots & \\ 0 & & & 1/L_M \end{pmatrix},
\tag{A10}
$$

where $L_j = L_{j1} + L_{j2}$. After transforming $\mathcal{C}_0$ by computing $U^t \mathcal{C}_0 U$ and truncating we get $\mathcal{C}_0'$.

While at this point we arrive at a valid representation of the dynamics, it is not the most convenient one because the capacitance matrix $\mathcal{C}_0'$ is in general nonzero in all its entries. We have found another change of variables, which is fairly local in that it only involves neighboring Brune stages, which brings the dynamics of the system into a more nearly diagonal form. We find that the transformation matrix T makes the Lagrangian of the system (i.e., both $\mathcal{C}_0'$ and M_0') band diagonal:

$$
T = \begin{pmatrix} 1 & & & & \\ -\frac{\sqrt{1+t_1^2}}{1-t_1} & -\frac{\sqrt{1+t_1^2}}{1-t_1} & & 0 & \\ & \frac{\sqrt{1+t_2^2}}{1-t_2} & \frac{\sqrt{1+t_2^2}}{1-t_2} & & \\ & & \ddots & \ddots & \\ 0 & & & (-1)^M\frac{\sqrt{1+t_M^2}}{1-t_M} & (-1)^M\frac{\sqrt{1+t_M^2}}{1-t_M} \end{pmatrix}.
\tag{A11}
$$

Applying T to $\mathcal{C}_0'$ and M_0' we get

$$
\mathcal{C} = T^t \mathcal{C}_0' T = \begin{pmatrix} C_J + C_1' & t_1 C_1' & & & \\ t_1 C_1' & t_1^2 C_1' + C_2' & \ddots & 0 & \\ & \ddots & \ddots & & \\ & 0 & & t_{M-1}^2 C_{M-1}' + C_M' & t_M C_M' \\ & & & t_M C_M' & t_M^2 C_M' + C_{M+1}' \end{pmatrix},
\tag{A12}
$$

$$
\mathbf{M_0} = T^t M_0' T = \begin{pmatrix} \frac{1}{L_1'} & \frac{1}{L_1'} & & & \\ \frac{1}{L_1'} & \frac{1}{L_1'}+\frac{1}{L_2'} & \frac{1}{L_2'} & & 0 \\ & \frac{1}{L_2'} & \frac{1}{L_2'}+\frac{1}{L_3'} & \ddots & \\ & & \ddots & \ddots & \\ & 0 & & \frac{1}{L_{M-1}'}+\frac{1}{L_M'} & \frac{1}{L_M'} \\ & & & \frac{1}{L_M'} & \frac{1}{L_M'} \end{pmatrix},
\tag{A13}
$$

where $C_j' = C_j/(1-t_j)^2$, $L_j' = L_{j2}(1-t_j)^2$.

A Lagrangian $\mathcal{L}_0$ (and equivalently a Hamiltonian $\mathcal{H}_S$) can be written as

$$
\mathcal{L}_0 = \tfrac{1}{2}\dot{\mathbf{\Phi}}^T \mathcal{C} \dot{\mathbf{\Phi}} - U(\mathbf{\Phi}), \quad \mathcal{H}_S = \tfrac{1}{2}\mathbf{Q}^T \mathcal{C}^{-1} \mathbf{Q} + U(\mathbf{\Phi}),
\tag{A14}
$$

where

$$
U(\mathbf{\Phi}) = -\left(\frac{\Phi_0}{2\pi}\right)^2 L_J^{-1} \cos(\varphi_J) + \frac{1}{2}\mathbf{\Phi}^T \mathbf{M_0} \mathbf{\Phi}. \tag{A15}
$$

$\mathbf{\Phi}$ is the vector of transformed (and truncated) coordinates of length $(M+1)$. φ_L is the phase across the Josephson junction. One can relate $\mathbf{\Phi}$ to the original branch fluxes in the Brune circuit by introducing an auxiliary vector $\mathbf{\Phi}'$ of length $(M+1)$

and keeping track of two coordinate transformations U and T applied as follows:

$$
\mathbf{\Phi}' = T\mathbf{\Phi},
\tag{A16}
$$

with

$$
\mathbf{\Phi}' = (\Phi_J, \Phi_1', \cdots, \Phi_M')
\tag{A17}
$$

$$
= U^t(\Phi_J, \mathbf{\Phi}_L)^t,
\tag{A18}
$$

where

$$
(\Phi_J, \mathbf{\Phi}_L) = (\Phi_J, \Phi_{12}, \Phi_{22}, \cdots, \Phi_{M2}, \Phi_{11}, \Phi_{21}, \cdots, \Phi_{M1})
\tag{A19}
$$

is the vector of fluxes of tree branches in the Brune circuit in Fig. (10), $\Phi_J = (\frac{\Phi_0}{2\pi})\varphi_J$, and

$$\Phi'_j = \frac{1}{\sqrt{1+t_j^2}}(\Phi_{j2} - t_j\Phi_{j1}) \tag{A20}$$

for $1 \leqslant j \leqslant M$. Note that $\Phi_1 = \Phi_J$. Here we assume that the vector $U^t(\Phi_J, \Phi_L)^t$ is truncated to its first $(M+1)$ rows before assignment to Φ'. From the truncated sector of the equation $\Phi' = U^t(\Phi_J, \Phi_L)^t$ we get the relations

$$\frac{1}{\sqrt{1+t_j^2}}(t_j\Phi_{j2} + \Phi_{j1}) = 0 \tag{A21}$$

for $1 \leqslant j \leqslant M$, which gives using Eq. (A20)

$$\Phi'_j = \sqrt{1+t_j^2}\,\Phi_{j2} \tag{A22}$$

for $1 \leqslant j \leqslant M$.

By Eq. (A16) we can write the jth component of Φ' for $1 \leqslant j \leqslant M$ as

$$\Phi'_j = (-1)^j \frac{\sqrt{1+t_j^2}}{1-t_j}(\Phi_j + \Phi_{j+1}). \tag{A23}$$

Hence by Eq. (A21) and Eq. (A22) we have

$$\Phi_{j1} = (-1)^{j+1}\frac{t_j}{1-t_j}(\Phi_j + \Phi_{j+1}), \tag{A24}$$

$$\Phi_{j2} = (-1)^j\frac{1}{1-t_j}(\Phi_j + \Phi_{j+1}) \tag{A25}$$

for $1 \leqslant j \leqslant M$. We see that the flux variables Φ_{j1} and Φ_{j2} of coupled inductor branches are functions of only two consecutive flux variables in the new coordinates Φ.

To treat resistors in Caldeira-Leggett formalism (in which each resistor is equivalent to a bath of harmonic oscillators with a smooth frequency spectrum) we will first compute the dissipation matrix $\mathcal{C}_Z(\omega)$ in Eq. (26) of [10]. We will then interpret the equation of motion $(\mathcal{C} + \mathcal{C}_Z)\ddot{\Phi} = -\frac{\partial U}{\partial \Phi}$ in Eq. (29) of [10] as an equation of motion Eq. (61) of [9] by taking the dissipative term to the right-hand side and writing (in the frequency domain) $\mathcal{C}\ddot{\Phi} = -\frac{\partial U}{\partial \Phi} - \omega^2\mathcal{C}_Z\Phi$. One can then relate $\mathbf{M}_d(\omega) = \omega^2\mathcal{C}_Z$ and $K(\omega) = \omega^2\bar{\mathbf{C}}_Z(\omega)$, where $\mathbf{M}_d$ and $K(\omega)$ are given in Eqs. (72)–(75) of [9]. Then coupling vectors $\bar{\mathbf{m}}$ are identical in both formalisms.

We treat each resistor separately. Applying Eq. (124) of [9] we get the contribution to the relaxation rate from the resistor R_j ($1 \leqslant j \leqslant M+1$):

$$\frac{1}{T_{1,j}} = 4|\langle 0|\bar{\mathbf{m}}_j \cdot \Phi|1\rangle|^2 J_j(\omega_{01})\coth\left(\frac{\hbar\omega_{01}}{2k_BT}\right). \tag{A26}$$

$|0,1\rangle$ are the qubit eigenlevels of the system Hamiltonian Eq. (A14). The vector $\bar{\mathbf{m}}_j$ [of length $(M+1)$] describes the coupling of the system to the environment representing resistor R_j. Note that our use of the non-normalized coupling vector $\bar{\mathbf{m}}_j$ and the flux vector Φ implies removal of the factor $\mu(\frac{\Phi_0}{2\pi})^2$ from the definition of the spectral function of the bath J in Eq. (93) of [9] [see Eqs. (A31) and (A34)].

For $1 \leqslant j \leqslant M$, using Eqs. (26)–(28) in [10] we compute

$$\bar{\mathbf{m}}_j = \begin{pmatrix} 0 \\ \vdots \\ 0 \\ \frac{(-1)^{j-1}C_j}{(1-t_j)} \\ \frac{(-1)^j C_{j+1}}{(1-t_{j+1})} + \frac{(-1)^{j-1}t_j C_j}{(1-t_j)} \\ \vdots \\ \frac{(-1)^{M-1}C_M}{(1-t_M)} + \frac{(-1)^{M-2}t_{M-1}C_{M-1}}{(1-t_{M-1})} \\ \frac{(-1)^{M-1}t_M C_M}{(1-t_M)} \end{pmatrix}, \tag{A27}$$

where $\bar{\mathbf{m}}_j$ are vectors of length $(M+1)$ and

$$\bar{\mathbf{C}}_{Z,j}(\omega) = -\frac{i\omega R_j}{1 + i\omega R_j\left(\sum_{k=j}^M C_k\right)}. \tag{A28}$$

We then have

$$K_j(\omega) = \omega^2\bar{\mathbf{C}}_{Z,j}(\omega) \tag{A29}$$

$$= \frac{i\omega^3 R_j}{1 + i\omega R_j\left(\sum_{k=j}^M C_k\right)}. \tag{A30}$$

Hence we obtain Eq. (8) of the main text:

$$J_j = \mathrm{Im}[K_j(\omega)] \tag{A31}$$

$$= \frac{\omega^3 R_j}{1 + \omega^2 R_j^2\left(\sum_{k=j}^M C_k\right)^2}. \tag{A32}$$

To treat the last resistor R_{M+1} we first replace C_{M+1} in the last row of the capacitance matrix by $1/(i\omega R_{M+1})$. This gives a term $-\frac{1}{R_{M+1}}\dot{\varphi}_M$ on the right-hand side of the Euler-Lagrange equations of motion [see Eq. (29) of [10]]. Such a simple replacement in one term is valid because the flux variable of this capacitive branch never appears as an independent variable. The reason for this special treatment of the last resistor is that, because of its shunt position, its resistance should be sent to infinity rather than zero to get the lossless limit; thus, $1/R_{M+1}$ should be the small parameter controlling dissipation. To perform a quantum treatment of all these dissipative contributions, we introduce a Caldeira-Leggett environment following the prescription of [9]. Following the notation of this treatment, we get a dissipation matrix for resistor R_{M+1}:

$$\mathbf{M}_d = K_{M+1}(\omega)\bar{\mathbf{m}}_{M+1}\bar{\mathbf{m}}_{M+1}^T, \tag{A33}$$

where $K_{M+1}(\omega) = \frac{i\omega}{R_{M+1}}$ and $\bar{\mathbf{m}}_{M+1} = (0\cdots01)^T$ is a vector with $(M+1)$ rows. We then have

$$J_{M+1}(\omega) = \mathrm{Im}[K_{M+1}(\omega)] = \frac{\omega}{R_{M+1}}, \tag{A34}$$

as stated in the main text. We note that this formalism has been thoroughly studied in previous work [27], where it was seen that it gives a good accounting for relaxation of nearly harmonic systems, obtaining results in agreement with classical arguments.

Finally, we note that, while the formulation given above appears to be highly singular for the case of any turns ratio

$t_i \to 1$ in both the Hamiltonian [Eqs. (A12) and (A13)] and the decay rates [Eqs. (A26) and (A27)], we have confirmed by examining other representations that all observable properties of the dynamics, such as ω_{01} and T_1, are smooth functions of t_i as it passes through unity.

1. Degenerate case

As discussed in the first part of this Appendix, Brune's algorithm may produce degenerate stages. In this text we will only consider the capacitive degenerate case. Such a case has appeared in the example circuit we studied as listed in Table II. We consider a degenerate case appearing at the kth stage. Such

a stage corresponds to the limit of $L'_k \to 0$ and $t_k \to 0$. To remove the singularity we define a transformation:

$$
T_d = \begin{pmatrix} 1 & & & & & \\ & \ddots & & & & \\ & & 1 & & & \\ \text{row} \quad (k+1) \to & & -1 & -1 & & \\ & & & & \ddots & \\ & & & & & -1 \end{pmatrix}. \quad \text{(A35)}
$$

Applying this transformation to the matrices $\mathbf{M_0}$ and $\mathcal{C}$ and removing the coordinate of the degenerate stage [this corresponds to the removal of the $(k+1)$th row and $(k+1)$th column from both matrices] we get

$$
T_d^t \mathbf{M_0} T_d = \begin{pmatrix} \frac{1}{L'_1} & \frac{1}{L'_1} & & & & & & & \\ \frac{1}{L'_1} & \frac{1}{L'_1}+\frac{1}{L'_2} & \frac{1}{L'_2} & & & & & & \mathbf{0} \\ & \frac{1}{L'_2} & \frac{1}{L'_2}+\frac{1}{L'_3} & \ddots & & & & & \\ & & \ddots & \ddots & & & & & \\ & & & & \frac{1}{L'_{k-1}}+\frac{1}{L'_{k+1}} & \frac{1}{L'_{k+1}} & & & \\ & & & & \frac{1}{L'_{k+1}} & \frac{1}{L'_{k+1}}+\frac{1}{L'_{k+2}} & \ddots & & \\ & & \mathbf{0} & & & \ddots & \ddots & & \\ & & & & & & & \frac{1}{L'_{M-1}}+\frac{1}{L'_M} & \frac{1}{L'_M} \\ & & & & & & & \frac{1}{L'_M} & \frac{1}{L'_M} \end{pmatrix}, \quad \text{(A36)}
$$

$$
T_d^t \mathcal{C} T_d = \begin{pmatrix} C_J+C'_1 & t_1 C'_1 & & & & & & \\ t_1 C'_1 & t_1^2 C'_1+C'_2 & \ddots & & & & \mathbf{0} & \\ & \ddots & \ddots & & & & & \\ & & & t_{k-1}^2 C'_{k-1}+(C'_{k+1}+C'_k) & t_{k+1}C'_{k+1} & & & \\ & & & t_{k+1}C'_{k+1} & t_{k+1}^2 C'_{k+1}+C'_{k+2} & \ddots & & \\ & & & & \ddots & \ddots & & \\ & & \mathbf{0} & & & & t_{M-1}^2 C'_{M-1}+C'_M & t_M C'_M \\ & & & & & & t_M C'_M & t_M^2 C'_M+C_{M+1} \end{pmatrix}. \quad \text{(A37)}
$$

Note that the matrices above are of size $M \times M$.

One needs to update also $\bar{\mathbf{m}}$ vectors. To do this we have to apply the transformation T_d to $\bar{\mathbf{m}}$ vectors and remove the entry corresponding to the degenerate coordinate (i.e., the $(k+1)$th row). Now we define some auxiliary vectors:

$$
\bar{\mathbf{m}}_a(j) = \begin{pmatrix} 0 \\ \vdots \\ 0 \\ (-1)^{j-1}\frac{C_j}{(1-t_j)} \\ \vdots \\ (-1)^{k-2}\frac{C_{k-1}}{(1-t_{k-1})} \\ (-1)^{k+1}\frac{C_{k+1}}{(1-t_{k+1})} \\ \vdots \\ (-1)^M \frac{C_M}{(1-t_M)} \\ 0 \end{pmatrix}, \quad j^{\text{th}} \text{ row} \longrightarrow \quad \text{(A38)}
$$

$$
\bar{\mathbf{m}}_b(j) = \begin{pmatrix} 0 \\ \vdots \\ 0 \\ (j+1)^{\text{th}} \text{ row} \longrightarrow (-1)^{j-1} \frac{t_j C_j}{(1-t_j)} \\ \vdots \\ (-1)^{k-2} \frac{t_{k-1} C_{k-1}}{(1-t_{k-1})} \\ (-1)^{k+1} \frac{t_{k+1} C_{k+1}}{(1-t_{k+1})} \\ \vdots \\ (-1)^M \frac{t_M C_M}{(1-t_M)} \end{pmatrix}, \tag{A39}
$$

$$
\bar{\mathbf{m}}_{C_k} = (0 \cdots 0 \, C_k \, 0 \cdots 0)^t, \tag{A40}
$$

where C_k is in the kth row. Now we can write coupling vector $\bar{\mathbf{m}}_j$ to the bath of the resistor R_j as a function of the vectors defined in Eqs. (A38)–(A40) as

$$
\bar{\mathbf{m}}_j = \bar{\mathbf{m}}_a(j) + \bar{\mathbf{m}}_b(j) + \bar{\mathbf{m}}_{C_k} \qquad \text{if } j \leqslant k, \tag{A41}
$$

$$
\bar{\mathbf{m}}_j = \bar{\mathbf{m}}_a(j) + \bar{\mathbf{m}}_b(j) \qquad \text{if } j > k. \tag{A42}
$$

Note that the vectors above are all of length M. Spectral densities $J_i(\omega)$ are the same as in the nondegenerate case [Eqs. (A32) and (A34)] for all resistors. Note also that dissipation treatment for the last resistor R_{M+1} is unaffected since C_{M+1} is untouched in Eq. (A37).

APPENDIX B: LOSSY FOSTER METHOD

Foster's theorem can be extended to responses with small loss [4]. We start with the partial fraction expansion for $Z(s)$:

$$
Z(s) = \sum_k \frac{R_k}{s - s_k}, \tag{B1}
$$

where R_k are residues and s_k are poles. Residues and poles come in complex conjugate pairs. If we define

$$
s_k = \xi_k + j\omega_k, \tag{B2}
$$

$$
R_k = a_k + jb_k. \tag{B3}
$$

Collecting terms corresponding to conjugate pairs,

$$
Z_k(s) = \frac{R_k}{s - s_k} + \frac{R_k^*}{s - s_k^*} \tag{B4}
$$

$$
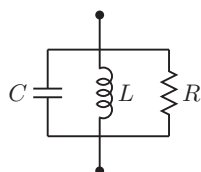= 2 \frac{a_k s - (a_k \xi_k + b_k \omega_k)}{s^2 - 2\xi_k s + \xi_k^2 + \omega_k^2}. \tag{B5}
$$

One can show that for physical circuits with small loss ξ_k and b_k are both small quantities [5]. Hence we can approximately write

$$
Z_k(s) \cong \frac{2a_k s}{s^2 - 2\xi_k s + \omega_k^2}. \tag{B6}
$$

The impedance function of the shunt resonant circuit as depicted in Fig. 14 is

$$
Z(s) = \frac{\frac{\omega_0 R}{Q} s}{s^2 + \frac{\omega_0}{Q} s + \omega_0^2}, \tag{B7}
$$

with

$$
\omega_0^2 = \frac{1}{LC}, \tag{B8}
$$

$$
Q = \omega_0 RC. \tag{B9}
$$

Hence we see that we can realize the function $Z_k(s)$ in Eq. (B6) by a circuit as in Fig. 14 with

$$
R = -a_k/\xi_k, \tag{B10}
$$

$$
\omega_0 = \omega_k, \tag{B11}
$$

$$
Q = -\omega_k/2\xi_k, \tag{B12}
$$

and the impedance in Eq. (B1) can be realized as in Fig. 15 by a series connection of stages in Fig. 14.

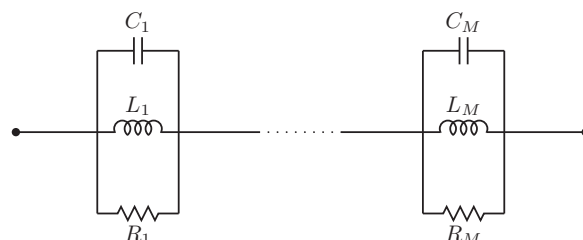FIG. 14. Generic shunt resonant stage in a lossy Foster circuit.

FIG. 15. Lossy Foster circuit.

[1] J. Bourassa, J. M. Gambetta, and A. Blais, in Proceedings of the APS March Meeting, 2011 (unpublished), Abstract No. Y29.00005.

[2] S. E. Nigg, H. Paik, B. Vlastakis, G. Kirchmair, S. Shankar, L. Frunzio, M. H. Devoret, R. J. Schoelkopf, and S. M. Girvin, Phys. Rev. Lett. **108**, 240502 (2012).

[3] R. M. Foster, Bell Systems Technical Journal **3**, 259 (1924).

[4] E. R. Beringer, in *Principles of Microwave Circuits*, edited by C. G. Montgomery, R. H. Dicke, and E. M. Purcell (Massachusetts Institute of Technology Radiation Laboratory, Cambridge, 1945), Vol. 8, Sec. 7.4, p. 215.

[5] E. A. Guillemin, *Synthesis of Passive Networks* (Krieger, Huntington, NY, 1977), Chap. 9.

[6] O. Brune, Ph.D. thesis, Massachusetts Institute of Technology, 1931.

[7] J. Bourassa, F. Beaudoin, Jay M. Gambetta, and A. Blais, Phys. Rev. A **86**, 013814 (2012)

[8] B. Gustavsen and A. Semlyen, in Proceedings of the IEEE Transactions on Power Delivery, 1999 (unpublished), Vol. 14, No. 3, pp. 1052–1061, available at http://www.sintef.no/Projectweb/VECTFIT/.

[9] G. Burkard, R. H. Koch, and D. P. DiVincenzo, Phys. Rev. B **69**, 064503 (2004).

[10] G. Burkard, Phys. Rev. B **71**, 144511 (2005).

[11] For example, see A. Blais, R. S. Huang, A. Wallraff, S. M. Girvin, and R. J. Schoelkopf, Phys. Rev. A **69**, 062320 (2004); J. Dempster, B. Fu, D. G. Ferguson, D. I. Schuster, and J. Koch, arXiv:1402.7310.

[12] C. Rigetti, J. M. Gambetta, S. Poletto, B. L. T. Plourde, J. M. Chow, A. D. Corcoles, J. A. Smolin, S. T. Merkel, J. R. Rozen, G. A. Keefe, M. B. Rothwell, M. B. Ketchen, and M. Steffen, Phys. Rev. B **86**, 100506(R) (2012).

[13] Ansys HFSS (High Frequency Structural Simulator), http://www.ansys.com.

[14] H. Paik, D. I. Schuster, L. S. Bishop, G. Kirchmair, G. Catelani, A. P. Sears, B. R. Johnson, M. J. Reagor, L. Frunzio, L. I. Glazman, S. M. Girvin, M. H. Devoret, and R. J. Schoelkopf, Phys. Rev. Lett. **107**, 240501 (2011).

[15] M. Reagor, H. Paik, G. Catelani, L. Sun, C. Axline, E. Holland, I. M. Pop, N. A. Masluk, T. Brecht, L. Frunzio, M. H. Devoret, L. I. Glazman, R. J. Schoelkopf, Appl. Phys. Lett. **102**, 192604 (2013).

[16] R. W. Newcomb, *Linear Multiport Synthesis* (McGraw-Hill, New York, 1966).

[17] D. Pozar, *Microwave Engineering* (Wiley, New York, 2005).

[18] M. K. Zinn, Bell System Technical Journal **31**, 378 (1952).

[19] W. Hendrickx, and T. Dhaene, IEEE Trans. Power Systems **21**, 441 (2006).

[20] B. Gustavsen and A. Semlyen, IEEE Trans. Power Systems **16**, 97 (2001).

[21] S. Ramo, J. R. Whinnery, and T. V. Duzer, *Fields and Waves in Communication Electronics* (Wiley, New York, 1967).

[22] For the purely harmonic system, the quantization discussed here was already treatable with the methods of B. Yurke and J. S. Denker, Phys. Rev. A **29**, 1419 (1984).

[23] The identification of this pole as the "qubit pole" is established by calculating the eigenmode of this pole and observing that it has its highest weight on the Josephson-junction branch of the circuit. Its mode frequency is also strongly dependent on L_J.

[24] But note a drawback of the approach of including the linear part of the Josephson response in the model circuit: in the resulting circuit there is no one branch circuit variable that represents the physical response of the Josephson device, unlike in our approach, where a single variable [φ_J of Eq. (3.2)] plays this role directly.

[25] I. M. Pop, K. Geerlings, G. Catelani, R. J. Schoelkopf, L. I. Glazman, and M. H. Devoret, Nature (London) **508**, 369 (2014).

[26] M. Stern, G. Catelani, Y. Kubo, C. Grezes, A. Bienfait, D. Vion, D. Esteve, and P. Bertet, Phys. Rev. Lett. **113**, 123601 (2014).

[27] D. P. DiVincenzo, F. Brito, and R. H. Koch, Phys. Rev. B **74**, 014514 (2006).